1-1-2004

# Effect of differential rotation on the maximum mass of neutron stars: Realistic nuclear equations of state

I.A. Morrison

T.W. Baumgarte

S.L. Shapiro

# EFFECT OF DIFFERENTIAL ROTATION ON THE MAXIMUM MASS OF NEUTRON STARS: REALISTIC NUCLEAR EQUATIONS OF STATE

Ian A. Morrison,[1] Thomas W. Baumgarte,[1,2] and Stuart L. Shapiro[2,3]

## ABSTRACT

The merger of binary neutron stars is likely to lead to differentially rotating remnants. In this paper, we survey several cold nuclear equations of state (EOSs) and numerically construct models of differentially rotating neutron stars in general relativity. For each EOS we tabulate maximum allowed masses as a function of the degree of differential rotation. We also determine effective polytropic indices and compare the maximum allowed masses with those for the corresponding polytropes. We consistently find larger mass increases for the polytropes, but even for the nuclear EOSs we typically find maximum masses 50% higher than the corresponding values for nonrotating (Tolman-Oppenheimer-Volkoff) stars. We evaluate our findings for the six observed binary neutron star (pulsar) systems, including the recently discovered binary pulsar J0737−3039. For each EOS we determine whether their merger could automatically lead to prompt collapse to a black hole, or whether the remnant can be supported against collapse by uniform rotation (possibly as a supramassive star) or differential rotation (possibly as a hypermassive star). For hypermassive stars, delayed collapse to a black hole is likely. For the most recent EOSs we survey the merger remnants can all be supported by rotation against prompt collapse, but their actual fate will depend on the nonequilibrium dynamics of the coalescence event. Gravitational wave observations of coalescing binary neutron stars may be able to distinguish these outcomes—no, delayed, or prompt collapse—and thereby constrain possible EOSs.

*Subject headings:* gravitation — relativity — stars: neutron — stars: rotation

## 1. INTRODUCTION

The remnant formed in the coalescence of binary neutron stars is likely to be differentially rotating (see, e.g., the dynamical simulations of Rasio & Shapiro 1992, 1994, 1999; Shibata & Uryū 2000, 2002; Faber et al. 2001, 2003; Oechslin et al. 2002; Shibata et al. 2003; see also the review of Baumgarte & Shapiro 2003). It is likely that differential rotation will play an important role in the dynamical stability of these remnants, since it can be very effective in increasing their maximum allowed mass (Baumgarte et al. 2000, hereafter BSS00; Lyford et al. 2003, hereafter LBS03).

Most neutron stars in binaries have individual gravitational masses close to 1.4 $M_\odot$ (see Table 2). Furthermore, most recent realistic nuclear equations of state predict a maximum allowed mass for nonrotating neutron stars in the range of about 1.7–2.3 $M_\odot$ (see Table 1). Taken together, these facts seem to suggest that the coalescence of binary neutron stars would lead to prompt collapse to a black hole. However, rotation, and especially differential rotation, can increase the maximum allowed mass significantly.[4]

The maximum allowed mass of *uniformly* rotating stars is limited by the spin rate at which the fluid at the equator moves on a geodesic (the Kepler limit); any further speedup would lead to mass shedding. Uniform rotation can therefore increase the maximum allowed mass by about 20% at most for very stiff equations of state (Cook et al.1992, 1994a, 1994b, hereafter CST1, CST2, and CST3, respectively; see also Table 1), which is not sufficient to stabilize remnants of binary neutron star coalescence. Uniformly rotating neutron stars with rest masses exceeding the maximum allowed rest mass for nonrotating stars (for the same equation of state) are referred to as *supramassive* neutron stars.

*Differential* rotation, however, is much more effective in increasing the maximum allowed mass. Unlike a uniformly rotating star, the rotation rate at the core of a differentially rotating star is not restricted to the maximum rotation rate at the equator, so that the core can be supported by rapid rotation without the equator having to exceed the Kepler limit. This effect was demonstrated in Newtonian gravitation by Ostriker et al. (1966) for white dwarfs and in general relativity by BSS00 for $n = 1$ polytropes. BSS00 also showed by way of illustration that stars with about 60% more mass than the maximum allowed mass of the corresponding nonrotating star can be dynamically stable against both radial and nonaxisymmetric modes. BSS00 refer to differentially rotating equilibrium configurations with rest masses exceeding the maximum rest mass of a uniformly rotating star as *hypermassive* neutron stars. LBS03 generalized the equilibrium results of BSS00 to other polytropic indices in the range $0.5 \le n \le 2.9$ and found that the largest relative increases in the maximum allowed mass can be found for polytropic indices close to $n = 1$. It is therefore not surprising that the hypermassive binary neutron star remnants formed in the $n = 1$ simulations of Shibata et al. (2003) do not collapse promptly to black holes unless they exceed the maximum nonrotating mass by more than about 70%. The merged remnants will be dynamically stable on a dynamical timescale. Viscous damping and magnetic braking of differential rotation will likely occur on a secular timescale (which is much greater than the dynamical timescale), leading to a delayed collapse and a delayed

---

[1] Department of Physics and Astronomy, Bowdoin College, Brunswick, ME 04011.

[2] Department of Physics, University of Illinois at Urbana-Champaign, Urbana, IL 61801.

[3] Department of Astronomy and NCSA, University of Illinois at Urbana-Champaign, Urbana, IL 61801.

[4] For coalescence from the innermost stable circular orbit, shear- and shock-induced thermal pressure, which can also increase the maximum allowed mass, is found to have a smaller effect.

TABLE 1
MAXIMUM MASS CONFIGURATIONS

| EOS | $M^{TOVa}$ | $M_0^{TOV}$ | $M^{UNI}$ | $M_0^{UNI}$ | $(\delta M_0/M_0)^{UNI}$ | $M^{DIF}$ | $M_0^{DIF}$ | $(\delta M_0/M_0)^{DIF}$ | $\hat{A}^{-1}$ |
|---|---|---|---|---|---|---|---|---|---|
| A[b] .............. | 1.66 | 1.92 | 1.95 | 2.24 | 0.17 | 2.62 | 2.90 | 0.51 | 0.7 |
| D[c] .............. | 1.65 | 1.89 | 1.95 | 2.22 | 0.18 | 2.71 | 3.02 | 0.60 | 0.7 |
| L[d] ............... | 2.70 | 3.23 | 3.27 | 3.87 | 0.20 | 4.45 | 5.04 | 0.56 | 0.7 |
| UT[e] ........... | 1.84 | 2.17 | 2.19 | 2.55 | 0.18 | 2.89 | 3.25 | 0.50 | 0.7 |
| FPS[f] .......... | 1.80 | 2.10 | 2.12 | 2.45 | 0.17 | 2.69 | 3.08 | 0.46 | 0.5 |
| APR[g] ......... | 2.20 | 2.67 | 2.46 | 3.10 | 0.16 | 2.95 | 3.50 | 0.31 | 0.3 |

[a] All masses are in units of $M_\odot$.
[b] Reid soft core (Pandharipande 1971).
[c] Model V (Bethe & Johnson 1974).
[d] Mean field (Pandharipande & Smith 1975).
[e] UV14 + TNI (Wiringa et al. 1988).
[f] UV14 + TNI (Lorenz et al. 1993).
[g] A18 + $\delta v$ + UIX* (Akmal et al. 1998).

burst of gravitational radiation (BSS00; Shapiro 2000; Cook et al. 2003; Liu & Shapiro 2003).

In this paper, we generalize the results of BSS00 and LBS03 to realistic equations of state. We construct differentially rotating neutron stars for a sample of six cold nuclear equations of state and tabulate their maximum allowed masses as a function of the degree of differential rotation. In addition, we identify an "effective" polytropic index for each of these equations of state and construct differentially rotating polytropes for these indices. We consistently find larger mass increases for the polytropes than for the nuclear equations of state, which is due to a drop in the maximum density for a rotating star with a large degree of differential rotation. However, even for nuclear equations of state we find increases in the maximum allowed rest mass of the order of about 50%, so that binary neutron star coalescence should often result in hypermassive neutron stars. We explicitly predict the fate of the six double neutron star binaries that have been identified to date, using the results of our equilibrium model calculations.

The paper is organized as follows. In § 2 we briefly summarize the numerical method and discuss the nuclear equations of state adopted in our calculations. In § 3 we present numerical results and compare our findings for nuclear equations of state with those for polytropes. We summarize our findings and discuss consequences for the six observed binary neutron star systems in § 4. In the Appendix we tabulate our numerical results. We adopt gravitational units and set $G = c = 1$.

## 2. CONSTRUCTING NUMERICAL MODELS

### 2.1. Equilibrium Models of Differentially Rotating Stars

As in BSS00 and LBS03, we use a modified version of the numerical code of CST1 to construct equilibrium models of differentially rotating neutron stars in general relativity. The code is based on similar numerical methods developed by Hachisu (1986) and Komatsu et al. (1989), and we refer to CST1 for details.

Constructing differentially rotating neutron star models requires choosing a rotation law $F(\Omega) = u^t u_\phi$, where $u^t$ and $u_\phi$ are components of the four-velocity $u^\alpha$ and $\Omega$ is the angular velocity. We follow CST1 and assume a rotation law $F(\Omega) = A^2(\Omega_c - \Omega)$, where the parameter $A$ has units of length and $\Omega_c$ is the central value of the angular velocity. Expressing $u^t$ and

$u_\phi$ in terms of $\Omega$ and metric potentials yields equation (42) of CST1, or

$$\Omega = \frac{\Omega_c}{1 + \hat{A}^{-2}\hat{r}^2 \sin^2\theta} \qquad (1)$$

in the Newtonian limit. Here we have rescaled $A$ and $r$ in terms of the equatorial radius $R_e$: $\hat{A} \equiv A/R_e$ and $\hat{r} \equiv r/R_e$. The parameter $\hat{A}$ is a measure of the degree of differential rotation and determines the length scale over which $\Omega$ changes. Since uniform rotation is recovered in the limit $\hat{A}^{-1} \to 0$, it is convenient to parameterize sequences by $\hat{A}^{-1}$. In the Newtonian limit the ratio between the central and equatorial angular velocities $\Omega_c/\Omega_e$ is related to $\hat{A}$ by $\Omega_c/\Omega_e = 1 + \hat{A}^{-2}$, but for relativistic configurations this relation holds only approximately.

We adopt this particular rotation law for convenience and for easy comparison with many other authors who have assumed the same law. However, as pointed out in LBS03, this rotation law approximates reasonably well the angular velocity profile of binary neutron star remnants in the fully relativistic dynamical simulations of Shibata & Uryū (2000, 2002) and the post-Newtonian simulations of Faber et al. (2001; see also Faber et al. 2003) for values of $\hat{A} \approx 1$. This suggests that the above rotation law may provide a reasonable parameterization of differential rotation profiles that one might expect to find in binary neutron star merger remnants.

We modified the numerical algorithm of CST1 by fixing the maximum interior density instead of the central density for each model. This change allows us to construct higher mass models in some cases, since the central density does not always coincide with the maximum density and hence may not specify a model uniquely.

For each equation of state and a given value of $\hat{A}$ we construct a sequence of models for each value of the maximum density by starting with a static, spherically symmetric star and then decreasing the ratio of the polar to equatorial radius, $\mathcal{R} \equiv R_p/R_e$, in decrements of 0.015. This sequence ends when we reach mass shedding (for large values of $\hat{A}$), when the code fails to converge or when $\mathcal{R} = 0$ (beyond which the star would become a toroid, a transition that current dynamical simulations do not indicate). For each of these sequences, the maximum achieved mass is recorded. We repeat this procedure for different values of the maximum density, which yields the maximum achieved mass as a function of maximum density. The maximum of this curve is the maximum allowed
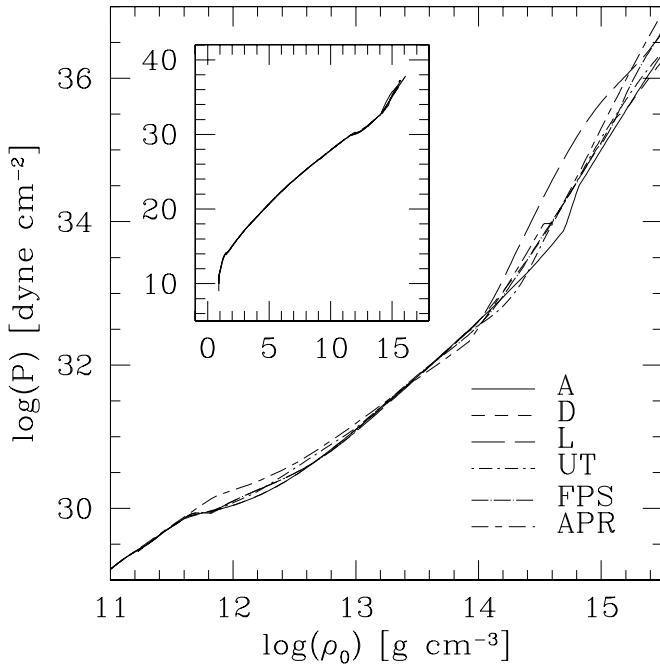
Fig. 1.—Pressure as a function of rest-mass density for the six nuclear equations of state adopted in this paper (see text and Table 1 for details).

mass for this particular equation of state and the chosen value of $\hat{A}$. In the Appendix we tabulate our numerical results for the equations of state described in § 2.2 and for $\hat{A}^{-1} = 0, 0.3, 0.5, 0.7,$ and $1.0$. Clearly, our maximum allowed masses are *lower limits* in the sense that even higher mass models may exist for other values of $\hat{A}$ or different differential rotation laws.

### 2.2. *Equations of State*

In this paper we adopt six cold, nuclear equations of state (EOSs), which are listed, together with numerical results, in Table 1. The first five, A, D, L, UT, and FPS, are adopted from CST3 (who in turn adopted the labeling of Friedman et al. 1986 for the first three EOSs). The last EOS, APR, was adapted from Akmal et al. (1998) by Ravenhall and Pandharipande (with the smooth matching between low and high density provided by G. Cook). In Figure 1 we plot the pressure $P$ as a function of the rest-mass density $\rho_0$ for these EOSs.

EOS A (Pandharipande 1971) models the interaction of neutrons at high densities with a Reid soft-core potential. EOS D is model V of Bethe & Johnson (1974). In EOS L the nucleon interaction is modeled in terms of a mean scalar field (Pandharipande & Smith 1975). Both EOSs UT (Wiringa et al. 1988) and FPS (Lorenz et al. 1993) are modern versions of an earlier EOS proposed by Friedman & Pandharipande (1981), which employs both two-body (U14) and three-body nucleon interactions (TNI). EOS UT improves the treatment of matter at high densities, while FPS describes the interactions in terms of a Skyrme model. EOS APR (Akmal et al. 1998) adopts a modern two-nucleon interaction (A18) together with boost corrections, as well as the UIX three-nucleon potential.

The different descriptions of nucleon interactions affect the EOS only at high densities. At low densities ($\rho_0 \lesssim 10^4$ g cm$^{-3}$), the EOSs employ the Feynman et al. (1949) EOS, joining onto the Baym et al. (1971) EOS up to neutron drip at $\rho_0 \approx 4 \times 10^{11}$ g cm$^{-3}$. Above neutron drip, EOSs A

and D join onto the Baym et al. (1971) EOS, while EOSs L and UT join onto the Negele & Vautherin (1973) EOS. EOS APR joins onto the FPS EOS below a number density of 0.1 fm$^{-3}$ ($\rho_0 = 1.26 \times 10^{14}$ g cm$^{-3}$).

All EOSs are read into our numerical code in tabular form, listing rest density $\rho_0$, the total energy density $\epsilon$, and the pressure $P$ at discreet points. Intermediate values of these quantities are computed by interpolation. Further details on the numerical implementation of these EOSs, including the fitting and tabulation, can be found in CST3.

### 3. RESULTS

Our numerical results are summarized in Table 1, where we list, for each equation of state, the nonrotating Tolman-Oppenheimer-Volkoff (TOV) maximum masses (both gravitational mass $M^{\text{TOV}}$ and rest mass $M_0^{\text{TOV}}$), the maximum masses for uniform rotation, and the maximum masses that we found in our survey of differential rotation. For convenience, we also list fractional mass increases with respect to the TOV maximum mass, as well as the parameter $\hat{A}^{-1}$ for which the maximum mass was encountered. More detailed results, with results for all values of $\hat{A}^{-1}$ considered in this paper, are tabulated in the Appendix.

The fractional mass increases are typically of the order of 50%. These increases are still large enough to support the remnant of a coalescing binary neutron star system in many cases (see § 4). However, they are noticeably below the increases for polytropic EOSs. LBS03 found that the fractional mass increases depend strongly on the polytropic index $n$, i.e., the stiffness of the EOS. For values of $n$ between 0.75 and 1.25, corresponding to moderately stiff EOSs, they found relative mass increases exceeding 100%. It is therefore somewhat surprising that the nuclear EOSs considered in this paper yield significantly smaller numbers.

To understand this result, we construct models of differentially rotating neutron stars for polytropic EOSs,

$$P = K\rho_0^{1+1/n}, \qquad (2)$$

where $K$ is a polytropic constant and $n$ is the polytropic index. For each nuclear EOS we identify an "effective" polytropic index $n_{\text{eff}}$ as follows. We first construct, for a nuclear EOS, the nonrotating (TOV) maximum mass model and compute for this model the central concentration $(\epsilon_c/\bar{\epsilon})_{\text{nucl}}$. Here $\epsilon_c$ is the central value of the energy density $\epsilon$, and we define the average energy density from

$$\bar{\epsilon} \equiv \frac{3M}{4\pi R^3}, \qquad (3)$$

where $M$ is the gravitational mass and $R$ is the circumferential radius. In Newtonian gravitation, this central condensation would correspond to a unique value of $n$. In general relativity, however, this is no longer the case. To identify the effective polytropic index $n_{\text{eff}}$, we therefore construct TOV maximum mass configurations for a large sample of polytropic indices, $n$ and compute their central condensation $(\epsilon_c/\bar{\epsilon})_{\text{poly}}$ as described above (see Table 1 in LBS03). We then interpolate between the polytropic values of the central condensation $(\epsilon_c/\bar{\epsilon})_{\text{poly}}$ to the desired nuclear value $(\epsilon_c/\bar{\epsilon})_{\text{nucl}}$ and thereby identify the effective polytropic index $n_{\text{eff}}$. We fix the polytropic constant $K$ in equation (2) by setting the mass of the polytropic maximum mass TOV model, which scales with $K^{n/2}$, equal to its counterpart for the corresponding nuclear EOS.
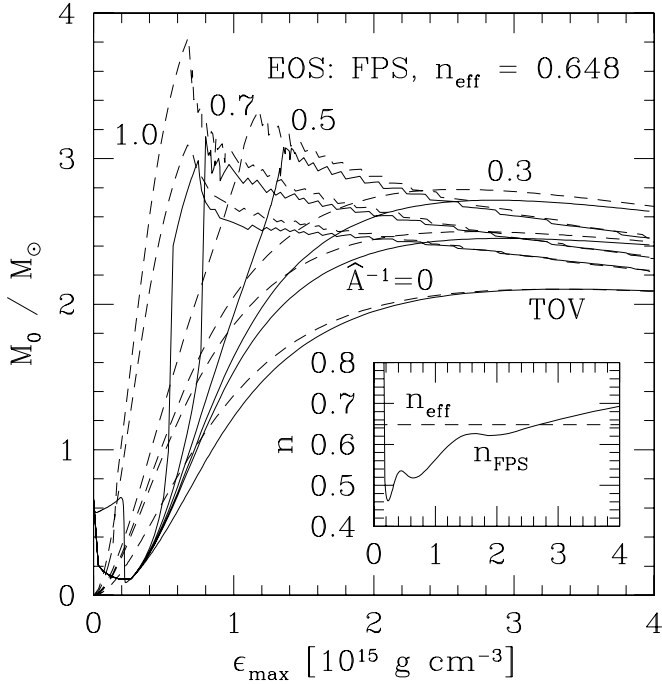
FIG. 2.—Maximum rest mass as a function of maximum density, $\epsilon_{max}$, for different values of $\hat{A}$. We include results for the FPS equation of state (*solid lines*), as well as for an $n = 0.648$ polytrope (*dashed lines*). The agreement is quite good for large values of $\epsilon_{max}$, but less so for smaller values of $\epsilon_{max}$ (for rotating as well as nonrotating stars). This can be understood in terms of the nuclear polytropic index $n_{FPS}$, which we show as a function of the density $\epsilon$ in the inset (*solid line*; as computed from eq. [5]). For small values of the density, the nuclear polytropic index $n_{FPS}$ drops significantly below the effective polytropic index $n_{eff}$ as computed from central condensation (*inset, dashed line*). The raggedness of some of the lines is a consequence of the finite step size in the parameter $\mathcal{R}$ that is varied along our constant density sequences and is a measure of the numerical error in our results.

We consistently find that the agreement between the nuclear EOS models and the corresponding polytropes is quite good (to within 10% or so) for those models that have a maximum density $\epsilon_{max}$ similar to the maximum mass TOV star. However, for larger degrees of differential rotation the maximum mass models shift to lower values of $\epsilon_{max}$ as the star become increasingly "toroidal" and bloated perpendicular to the rotation axis. We show this effect for EOS FPS in Figure 2, and we find qualitatively identical results for all other EOSs (see also Fig. 1 in BSS00).

This behavior can be understood by computing, as an alternative to our construction above, a "nuclear" polytropic index from the slope of the graphs in Figure 1. Using the adiabatic index,

$$\Gamma = \frac{\partial \ln P}{\partial \ln \rho_0}, \qquad (4)$$

we define a nuclear polytropic index by

$$n_{nucl} = \frac{1}{\Gamma - 1}. \qquad (5)$$

Clearly, this index is a function of density, and its value reflects different interactions dominating different density regimes. Across phase transitions, $n_{nucl}$ can even change discontinuously. We include a plot of $n_{FPS}$ as a function of the density $\epsilon$ in Figure 2 (*inset*).

For a polytropic EOS, on the other hand, $n$ is strictly independent of the density. We can therefore expect good agreement between polytropic and nuclear models only as long as $n_{eff}$ is close to $n_{nucl}$ for most of the matter in the star. As can be seen in Figure 2 (*inset*), $n_{eff}$ is very close to $n_{FPS}$ for densities in the range $(1.5-3) \times 10^{15}$ g cm$^{-3}$. This coincides quite well with the regime of maximum densities in equilibrium models for which the agreement between the polytropic and nuclear models is fairly good. For lower densities, $n_{FPS}$ drops significantly below $n_{eff}$, and it is therefore not surprising that stellar models with maximum densities in this regime no longer agree very well.

For all other EOSs we find very similar results. In all cases, the nuclear adiabatic index $n_{nucl}$ is very close to the effective polytropic index $n_{eff}$ (as determined from the central condensation) for densities close to the maximum density of the maximum mass TOV star. Matter in this density regime dominates the structure of the star for uniform and moderate degrees of differential rotation, leading to good agreement between nuclear and polytropic models. For larger degrees of differential rotation, the star becomes increasingly "toroidal" and bloated, and the maximum density shifts to smaller values. As a consequence, the star is dominated by matter at smaller densities, for which $n_{nucl}$ no longer agrees with $n_{eff}$. Accordingly, the results for the polytropic models are no longer in good agreement with the nuclear models.

## 4. SUMMARY AND DISCUSSION

We have constructed models of differentially rotating neutron stars in general relativity for a sample of realistic nuclear equations of state. We find that their maximum rest masses are typically larger than those of nonrotating neutron stars by about 50%. This increase is significantly less than the increases for moderately stiff polytropic equations of state (cf. LBS03). This deviation can be explained in terms of a drop in the maximum density for stars with large degrees of differential rotation. At these smaller densities, the stiffness of the nuclear equation of state, as determined from equation (5), is different from that at the maximum density of maximum mass nonrotating or uniformly rotating stars. Consequently, predictions based on simple polytropic models break down for sufficiently large degrees of differential rotation.

Even a mass increase of 50% may well be sufficient to support the remnant of binary neutron star coalescence. In fact, our findings can be used to predict possible fates for the six known double neutron star binaries as listed in Table 2. For four of those, B1524+12, B1913+16, B2127+11C, and the newly discovered binary J0737−3039, the individual gravitational masses are known to high accuracy (Thorsett & Chakrabarty 1999; Burgay et al. 2003; Lyne et al. 2004). For the two remaining ones, J1518+4904 and B2303+46, the orbital inclination is unknown, so that the combined gravitational mass is known to much higher accuracy than the individual masses. Assuming no mass loss during the coalescence and merger (Faber et al. 2003), the total rest mass of the binary is conserved (the total gravitational mass is not conserved because of neutrino and gravitational radiation losses). The rest mass corresponding to a particular gravitational mass depends on the equation of state, as is shown in Figure 3 for the four binaries with well-established individual masses.

The total rest mass $M_0^{tot}$ of the binary is an indicator of the fate of the merger remnant. If the total rest mass is less than the maximum (nonrotating) TOV mass $M_0^{TOV}$, then the

TABLE 2
MASS DATA FOR DOUBLE NEUTRON STAR BINARIES

| Binary | Gravitational Masses ($M_\odot$) | Combined Mass ($M_\odot$) | A[a] | D | L | UT | FPS | APR |
|---|---|---|---|---|---|---|---|---|
| J1518+4904[b,c] .......... | 1.05, 1.56 | 2.62 ± 0.07 | BH | HNS | NS | HNS | HNS | SNS |
| B1534+12[c] ............... | 1.339, 1.339 | 2.678 ± 0.012 | BH | HNS | NS | HNS | HNS | SNS |
| B1913+16[c] ............... | 1.3874, 1.4411 | 2.8285 ± 0.0014 | BH | BH | NS | HNS | BH | HNS |
| B2127+11C[c]............. | 1.349, 1.363 | 2.7122 ± 0.0006 | BH | HNS | NS | HNS | HNS | SNS |
| B2303+46[b,c]............. | 1.30, 1.34 | 2.64 ± 0.05 | BH | HNS | NS | HNS | HNS | SNS |
| J0737−3039[d] ........... | 1.250, 1.337 | 2.588 ± 0.003 | HNS | HNS | NS | HNS | HNS | SNS |

[a] Possible outcomes of binary merger for each equation of state according to computed total rest mass: NS, neutron star; SNS, supramassive neutron star; HNS, hypermassive neutron star; BH, black hole.

[b] For these systems the binary inclination angle has not been determined precisely, so that the combined mass is known to much higher accuracy than the individual neutron star masses.

[c] Thorsett & Chakrabarty (1999). Lower and upper limits for combined mass are 95% central limits.

[d] Lyne et al. (2004).

remnant can be supported against gravitational collapse even without rotation. This possibility is identified by "NS" in Table 2. If $M_0^{\mathrm{tot}}$ is greater than $M_0^{\mathrm{TOV}}$, but less than the maximum mass of uniformly rotating stars $M_0^{\mathrm{UNI}}$, then the merger could lead to a supramassive star, supported by uniform rotation (denoted by "SNS" in Table 2). If $M_0^{\mathrm{tot}}$ is greater than $M_0^{\mathrm{UNI}}$ but less than the maximum mass we find for differentially rotating stars $M_0^{\mathrm{DIF}}$, merger may lead to a hypermassive neutron star supported by differential rotation (denoted by "HNS"). If, finally, $M_0^{\mathrm{tot}}$ is greater than $M_0^{\mathrm{DIF}}$, the remnant will

promptly collapse to a black hole ("BH"). Clearly, these limits are only approximations, and the true outcome will depend not only on the mass and EOS but also on the non-equilibrium dynamics of the merger.

Since the rest masses of the observed binaries depend on the equation of state, so do the possible fates. Moreover, since all binary neutron star systems known to date have similar total masses, their fate, for a given equation of state, is presumably similar. In Table 2, the predictions for four of the six binaries are identical; only the high-mass binary B1913+16 and the
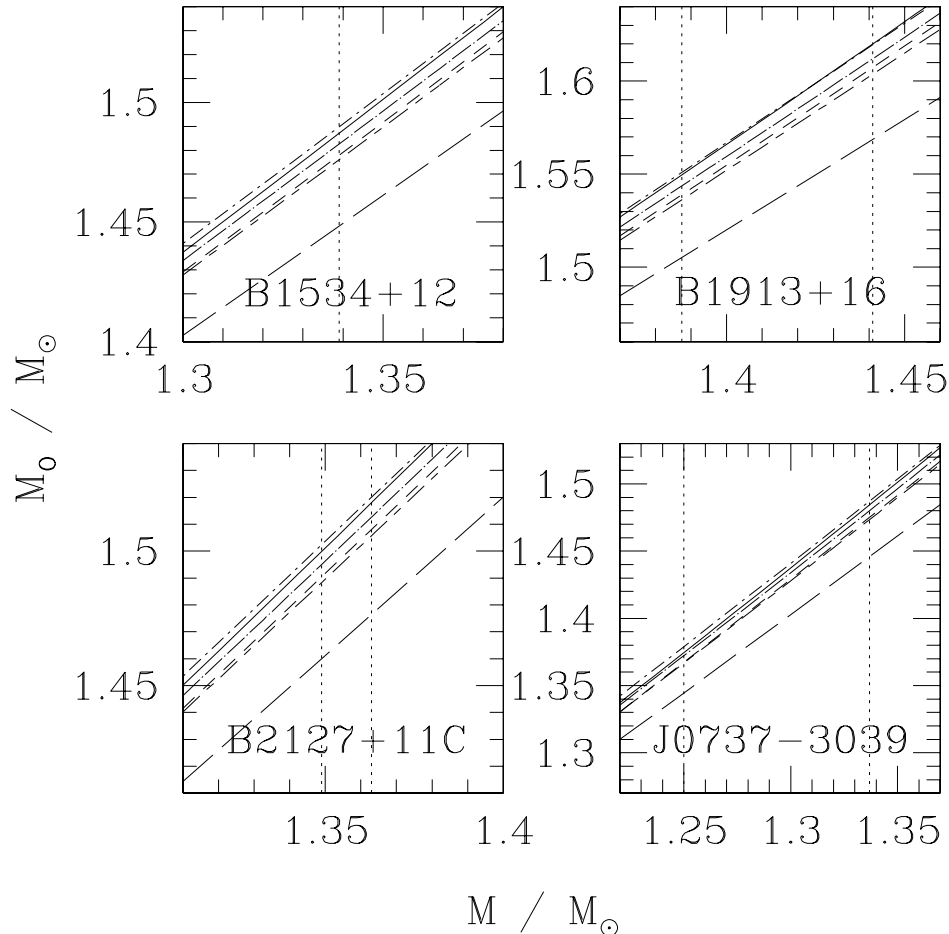


FIG. 3.—Rest mass $M_0$ as a function of gravitational mass $M$ for the six nuclear equations of state (labeled as in Fig. 1). The vertical lines mark the gravitational mass of the individual neutron stars in those four binary neutron star systems for which the individual masses have been well established.

low-mass binary J0737−3039 show any differences for some of the equations of state.

Table 2 suggests two immediate conclusions. For all the recent equations of state we survey and for all binaries except for B1913+16, the coalescence is likely to lead to a neutron star. For three of the six equations of state, the merger of these binaries could lead to a hypermassive neutron star. Unlike supramassive neutron stars, hypermassive neutron stars last only a fairly short time, until magnetic fields or viscous dissipation drive the objects toward uniform rotation, triggering a delayed collapse to a black hole (see BSS00; Duez et al. 2004).

Second, Table 2 shows that the outcome of binary neutron star coalescence is quite sensitive to the equation of state. This means that *the observational identification of a merger remnant, and its possible delayed collapse to a black hole, could place a tight constraint on the equation of state*. Advanced Laser Interferometer Gravitational Wave Observatory (LIGO)

and other new gravitational wave laser interferometers may be able to observe binary neutron star coalescence. Comparing the most recent equations of state, UT, FPS, and APR, it seems likely that the coalescence will lead to a rotationally supported neutron star. Observation of the remnant's delayed collapse to a black hole, or its absence, would then help to put constraints on possible equations of state.

# APPENDIX

## NUMERICAL RESULTS FOR MAXIMUM MASSES

In Tables 3–8 we list values for the maximum rest masses for uniformly and differentially rotating polytropes. For each equation of state we tabulate the differential rotation parameter $\hat{A}^{-1}$, the maximum energy density $\epsilon_{max}$, the ratio of the central and equatorial angular velocity $\Omega_c/\Omega_e$, the ratio between polar and equatorial radii $R_p/R_e$, the ratio of the (relativistic) rotational kinetic energy and the gravitational binding energy $T/|W|$, the maximum rest mass $M_0^{max}$, and the fractional rest mass increase $(\delta M_0/M_0)$. We also construct differentially rotating polytropes for effective polytropic indices $n_{eff}$ as described in § 3 and listed in each table heading. We include in the tables the fractional mass increases $(\delta M_0/M_0)_{poly}$ for these polytropes.

All models are computed with 64 zones both in the radial and angular direction and with the Legendre polynomial expansion truncated at $l = 16$ (see CST1 for details of the numerical implementation). The error in the ratio $R_p/R_e$ is determined by our step size of 0.015 in this ratio (see § 2.1). We finally note that highly toroidal configurations depend very sensitively on the input parameters, so that those mass increases depend on the parameters adopted in our restricted survey.

TABLE 3
A: $M_0^{TOV} = 1.92\ M_\odot$, $\bar{\epsilon}/\epsilon_c = 0.326$, $n_{eff} = 0.621$

| $\hat{A}^{-1}$ | $\epsilon_{max}/10^{15}$ g cm$^{-3}$ | $\Omega_c/\Omega_e$ | $R_p/R_e$ | $T/|W|$ | $M_0^{max}/M_\odot$ | $(\delta M_0/M_0)$ | $(\delta M_0/M_0)_{poly}$ |
|---|---|---|---|---|---|---|---|
| 0.0.................. | 3.55 | 1.000 | 0.565 | 0.120 | 2.24 | 0.17 | 0.19 |
| 0.3.................. | 3.45 | 1.465 | 0.460 | 0.180 | 2.50 | 0.30 | 0.34 |
| 0.5.................. | 1.87 | 2.026 | 0.415 | 0.227 | 2.69 | 0.40 | 0.56 |
| 0.7.................. | 0.938 | 2.448 | 0.220 | 0.293 | 2.90 | 0.51 | 0.76 |
| 1.0.................. | 1.12 | 3.584 | 0.310 | 0.235 | 2.34 | 0.22 | 0.43 |

TABLE 4
D: $M_0^{TOV} = 1.89\ M_\odot$, $\bar{\epsilon}/\epsilon_c = 0.284$, $n_{eff} = 0.738$

| $\hat{A}^{-1}$ | $\epsilon_{max}/10^{15}$ g cm$^{-3}$ | $\Omega_c/\Omega_e$ | $R_p/R_e$ | $T/|W|$ | $M_0^{max}/M_\odot$ | $(\delta M_0/M_0)$ | $(\delta M_0/M_0)_{poly}$ |
|---|---|---|---|---|---|---|---|
| 0.0.................. | 2.73 | 1.000 | 0.565 | 0.110 | 2.22 | 0.18 | 0.18 |
| 0.3.................. | 2.64 | 1.344 | 0.505 | 0.153 | 2.41 | 0.28 | 0.28 |
| 0.5.................. | 1.51 | 1.963 | 0.385 | 0.235 | 2.95 | 0.56 | 0.55 |
| 0.7.................. | 0.884 | 2.455 | 0.275 | 0.279 | 3.02 | 0.60 | 1.0 |
| 1.0.................. | 0.774 | 3.463 | 2.965 | 0.224E−07 | 2.97 | 0.57 | 0.66 |

TABLE 5
L: $M_0^{TOV} = 3.23\ M_\odot$, $\bar{\epsilon}/\epsilon_c = 0.339$, $n_{eff} = 0.586$

| $\hat{A}^{-1}$ | $\epsilon_{max}/10^{15}$ g cm$^{-3}$ | $\Omega_c/\Omega_e$ | $R_p/R_e$ | $T/|W|$ | $M_0^{max}/M_\odot$ | $(\delta M_0/M_0)$ | $(\delta M_0/M_0)_{poly}$ |
|---|---|---|---|---|---|---|---|
| 0.0.................. | 1.26 | 1.000 | 0.550 | 0.134 | 3.87 | 0.20 | 0.19 |
| 0.3.................. | 1.13 | 1.505 | 0.425 | 0.210 | 4.52 | 0.40 | 0.37 |
| 0.5.................. | 0.498 | 1.970 | 0.320 | 0.273 | 4.78 | 0.48 | 0.52 |
| 0.7.................. | 0.378 | 2.502 | 0.010 | 0.298 | 5.04 | 0.56 | 0.69 |
| 1.0.................. | 0.374 | 3.464 | 0.025 | 0.272 | 4.06 | 0.26 | 0.35 |

TABLE 6

UT: $M_0^{\mathrm{TOV}} = 2.17\ M_\odot$, $\bar{\epsilon}/\epsilon_c = 0.321$, $n_{\mathrm{eff}} = 0.635$

| $\hat{A}^{-1}$ | $\epsilon_{\max}/10^{15}$ g cm$^{-3}$ | $\Omega_c/\Omega_e$ | $R_p/R_e$ | $T/|W|$ | $M_0^{\max}/M_\odot$ | $(\delta M_0/M_0)$ | $(\delta M_0/M_0)_{\mathrm{poly}}$ |
|---|---|---|---|---|---|---|---|
| 0.0.................. | 2.73 | 1.000 | 0.565 | 0.122 | 2.56 | 0.18 | 0.19 |
| 0.3.................. | 2.66 | 1.455 | 0.460 | 0.182 | 2.86 | 0.32 | 0.33 |
| 0.5.................. | 2.02 | 2.145 | 0.490 | 0.195 | 2.91 | 0.34 | 0.57 |
| 0.7.................. | 0.763 | 2.441 | 0.220 | 0.293 | 3.25 | 0.50 | 0.81 |
| 1.0.................. | 0.744 | 3.468 | 0.010 | 0.273 | 2.97 | 0.37 | 0.47 |

TABLE 7

FPS: $M_0^{\mathrm{TOV}} = 2.10\ M_\odot$, $\bar{\epsilon}/\epsilon_c = 0.316$, $n_{\mathrm{eff}} = 0.648$

| $\hat{A}^{-1}$ | $\epsilon_{\max}/10^{15}$ g cm$^{-3}$ | $\Omega_c/\Omega_e$ | $R_p/R_e$ | $T/|W|$ | $M_0^{\max}/M_\odot$ | $(\delta M_0/M_0)$ | $(\delta M_0/M_0)_{\mathrm{poly}}$ |
|---|---|---|---|---|---|---|---|
| 0.0.................. | 2.92 | 1.000 | 0.565 | 0.117 | 2.45 | 0.17 | 0.19 |
| 0.3.................. | 2.83 | 1.440 | 0.475 | 0.172 | 2.72 | 0.29 | 0.32 |
| 0.5.................. | 1.36 | 1.942 | 0.360 | 0.248 | 3.08 | 0.46 | 0.59 |
| 0.7.................. | 0.836 | 2.446 | 0.275 | 0.278 | 3.06 | 0.45 | 0.82 |
| 1.0.................. | 0.748 | 3.469 | 0.010 | 0.275 | 2.99 | 0.42 | 0.47 |

TABLE 8

APR: $M_0^{\mathrm{TOV}} = 2.67\ M_\odot$, $\bar{\epsilon}/\epsilon_c = 0.377$, $n_{\mathrm{eff}} = 0.495$

| $\hat{A}^{-1}$ | $\epsilon_{\max}/10^{15}$ g cm$^{-3}$ | $\Omega_c/\Omega_e$ | $R_p/R_e$ | $T/|W|$ | $M_0^{\max}/M_\odot$ | $(\delta M_0/M_0)$ | $(\delta M_0/M_0)_{\mathrm{poly}}$ |
|---|---|---|---|---|---|---|---|
| 0.0.................. | 2.44 | 1.000 | 0.580 | 0.132 | 3.10 | 0.16 | 0.20 |
| 0.3.................. | 1.77 | 1.553 | 0.445 | 0.210 | 3.49 | 0.31 | 0.42 |
| 0.5.................. | 1.06 | 1.970 | 0.370 | 0.245 | 3.34 | 0.25 | 0.76 |
| 0.7.................. | 0.770 | 2.449 | 0.280 | 0.275 | 3.19 | 0.19 | 0.46 |
| 1.0.................. | 0.691 | 3.451 | 0.010 | 0.276 | 3.12 | 0.17 | 0.81 |

REFERENCES

Akmal, A., Pandharipande, V. R., & Ravenhall, D. G. 1998, Phys. Rev. C, 58, 1804
Baumgarte, T. W., & Shapiro, S. L. 2003, Phys. Rep., 376, 41
Baumgarte, T. W., Shapiro, S. L., & Shibata, M. 2000, ApJ, 528, L29 (BSS00)
Baym, G., Bethe, H. A., & Pethick, C. J. 1971, Nucl. Phys. A, 175, 225
Baym, G., Pethick, C. J., & Sutherland, P. 1971, ApJ, 170, 299
Bethe, H. A., & Johnson, M. B. 1974, Nucl. Phys. A, 230, 1
Burgay, M., et al. 2003, Nature, 426, 531
Cook, G. B., Shapiro, S. L., & Teukolsky, S. A. 1992, ApJ, 398, 203 (CST1)
———. 1994a, ApJ, 422, 227 (CST2)
———. 1994b, ApJ, 424, 823 (CST3)
Cook, J. N., Shapiro, S. L., & Stephens, B. C. 2003, ApJ, 599, 1272
Duez, M. D., Liu, Y. Y., Shapiro, S. L., & Stephens, B. C. 2004, Phys. Rev. D, in press (astro-ph/0402502)
Faber, J. A., Grandclément, P., & Rasio, F. A. 2003, Phys. Rev. D, submitted (gr-qc/0312097)
Faber, J. A., Rasio, F. A., & Manor, J. B. 2001, Phys. Rev. D, 63, 044012
Feynman, R. P., Metropolis, N., & Teller, E. 1949, Phys. Rev., 75, 1561
Friedman, J. F., Ipser, J. R., & Parker, L. 1986, ApJ, 304, 115
Friedman, J. F., & Pandharipande, V. R. 1981, Nucl. Phys. A, 361, 502
Hachisu, I. 1986, ApJS, 61, 479
Komatsu, H., Eriguchi, Y., & Hachisu, I. 1989, MNRAS, 237, 355

Liu, Y. T., & Shapiro, S. L. 2003, Phys. Rev. D, 69, 044009
Lorenz, C. P., Ravenhall, D. G., & Pethick, C. J. 1993, Phys. Rev. Lett., 70, 379
Lyford, N. D., Baumgarte, T. W., & Shapiro, S. L. 2003, ApJ, 583, 410 (LBS03)
Lyne, A. G., et al. 2004, Science, 303, 1153
Negele, J. W., & Vautherin, D. 1973, Nucl. Phys. A, 207, 298
Oechslin, R., Rosswog, S., & Thielemann, F.-K. 2002, Phys. Rev. D, 65, 103005
Ostriker, J. P., Bodenheimer, P., & Lynden-Bell, D. 1966, Phys. Rev. Lett., 17, 816
Pandharipande, V. R. 1971, Nucl. Phys. A, 174, 641
Pandharipande, V. R., & Smith, R. A. 1975, Phys. Lett. B, 59, 15
Rasio, F. A., & Shapiro, S. L. 1992, ApJ, 401, 226
———. 1994, ApJ, 432, 242
———. 1999, Classical Quantum Gravity, 16, R1
Shapiro, S. L. 2000, ApJ, 544, 397
Shibata, M., & Uryū, K. 2000, Phys. Rev. D, 61, 064001
———. 2002, Prog. Theor. Phys., 107, 265
Shibata, M., Uryū, K., & Taniguchi, K. 2003, Phys. Rev. D, 68, 084020
Thorsett, S. E., & Chakrabarty, D. 1999, ApJ, 512, 288
Wiringa, R. B., Fiks, V., & Fabrocini, A. 1988, Phys. Rev. C, 38, 1010